Neutron-scattering study of the incommensurate phase transition of Rb_2ZnBr_4

C. J. de Pater
Laboratorium voor Technische Natuurkunde, Werkgroep Fysische Kristallografie, Technische Hogeschool, Delft, Netherlands

C. van Dijk
Netherlands Energy Research Foundation, ECN, Petten (NH), Netherlands

(Received 23 February 1978)

A neutron-scattering study is presented of the modulation phase transition, at $T_c = 82°C$, of Rb_2ZnBr_4. A derivation is given of the structure factor for the diffuse scattering that appears near the transition which is described with a complex order parameter, i.e., amplitude as well as phase fluctuations of the order parameter are treated. The displacive character of the modulation is established and the spectra of the critical diffuse scattering in the high-temperature phase are interpreted with the help of a soft-phonon model. The soft excitations are overdamped near T_c and become underdamped only far above the transition temperature. The frequency of these excitations remains very low, i.e., below 0.1 THz. The acoustical branches and one optical dispersion branch along crystal axes were measured, at room temperature, and found to be stable in the entire temperature region of interest. In the low-temperature phase a broad diffuse scattering distribution was found around the satellite reflections. The spectra of this diffuse scattering are overdamped and no propagating excitations, corresponding to a soft mode, were observed in the low-temperature phase. Since phase or amplitude fluctuations of the order parameter will give rise to scattering close to the satellite positions our data provide evidence for an overdamped phase or amplitude excitation branch.

I. INTRODUCTION

The object of this paper is the study of dynamical aspects of the modulation phase transition and ground state of the compound Rb_2ZnBr_4. In the high-temperature phase the structure of Rb_2ZnBr_4 can be described like that of any crystal, on a three-dimensional lattice. However, below 82°C extra reflections appear in the diffraction pattern that can only be explained by introducing a fourth index m, besides h, k, l. With the help of the four Miller indices h, k, l, m, the reciprocal vector of a satellite reflection can be written

$$\vec{\tau} = (h + m k_{0,a})\vec{a}^* + (k + m k_{0,b})\vec{b}^* + (l + m k_{0,c})\vec{c}^* ,$$

where $k_{0,a}$, $k_{0,b}$, and $k_{0,c}$ are the components of the modulation wave vector $\vec{k}_0$.

In real space, the cause of these reflections must be sought in an extra coordinate that is required to describe the crystal's periodicity. The structure remains perfectly ordered, as required for a crystal, but it is only periodic on four coordinates. de Wolff[1] has given an extensive treatment of the consequences of this phenomenon for the symmetry of the present crystal. Here we will limit ourselves to a definition of the structure

$$\vec{r}_{\kappa l} = \vec{r}_l + \vec{r}_\kappa + \vec{A}_\kappa \sin(\vec{k}_0 \cdot \vec{r}_l + \phi_\kappa) , \qquad (1)$$

where $\vec{r}_l$ is the position vector of the unit cell and $\vec{r}_\kappa$ that of atom of type κ in the cell.

The phase of the modulation wave appears here as the fourth coordinate, provided that $\vec{k}_0$ is irrational with respect to the reference lattice. This reference lattice, given by $\{\vec{r}_l, \vec{r}_\kappa\}$ remains prominent at all temperatures. So we consider the modulation as a perturbation of a three-dimensional periodic structure.

The motivation to study such modulated compounds is mainly founded in the departure from three-dimensional periodicity. An additional interesting point is that the modulation phase may be regarded as a generalization of a ferroelectric or antiferroelectric phase. Perhaps, the modulated structure can be explained by extending existing models of ferroelectrics.[2] On the other hand, there will be completely new phenomena in a modulated crystal, e.g., the excitations corresponding to fluctuations of the phase of the wave. This is possible because a phase shift corresponds to small atom shifts; the phase of the wave is in no way fixed to the basic structure lattice. The phase fluctuations at the modulation wave vector require no energy, so one expects a new vibrational branch that goes to zero frequency at the satellite position.

The present study concerns a particular member of the A_2BX_4 family ($A = NH_4$, K, Rb; B = Zn, Co, Se; X = Br, Cl, O). Several structures in this family are modulated whereas others have rational superstructures ($k_0 = \frac{1}{4}$ or $\frac{1}{3}$).

The average structure has been determined from a neutron-diffraction powder diagram. It fits very

well in the β-K_2SO_4 model. So we may say that there are chains of Rb ions and of alternating $ZnBr_4$ tetrahedra and Rb ions in the c direction, which is the pseudohexagonal axis. This average structure shows translations of the Rb atoms and the tetrahedra perpendicular to the mirror plane and rotations of the tetrahedra around the c axis, resulting in an amplitude of all atomic displacements at room temperature of about 0.25 Å. We described the average structure in space group $Pcmn$ with cell constants: $a = 13.343$ Å, $b = 7.656$ Å, $c = 9.708$ Å, $k_0 = 0.292c^*$ (the modulation wavelength is about 33 Å).

Since the covalent Zn-Br bonds are much stronger than the other bonds, we expect only six degrees of freedom for a tetrahedron in the lattice modes. This yields, together with the degrees of freedom of the Rb ions, 48 modes for the external vibrations. The resulting complexity of the dynamics of Rb_2ZnBr_4 makes a full solution of the lattice dynamics, as well as a complete measurement of the dispersion branches impossible. In this respect, our study has to be limited to a few aspects of the dynamical problem. We shall sometimes refer to Na_2CO_3, the structure of which is also related to the family of $A_2BX_{3,4}$ structures, which we now consider.

The Na_2CO_3 structure has been determined,[3] and we know that the modulation is of the type described in (1). In other cases the situation is not quite clear yet, mainly because higher-order satellites are lacking. Consequently, a disorder modulation is possible, which means that going from cell to cell (along the direction of the modulation wave vector) the atoms are shifted from a basic lattice, but can only be found in two positions. The probability for the occupation of these positions may again be modulated sinusoidally, with the period of the modulation.

The present study describes measurements in the temperature range of 20 to 200°C, in which $\vec{k}_0$ is constant. However, after completing these measurements it was found that at lower temperatures k_0 increases continuously and jumps at −80°C from $0.308c^*$ to the commensurate value of $\frac{1}{3}$, thus undergoing a so-called lock-in transition.

II. EXPERIMENTAL

The neutron-scattering experiments were done with a triple axis spectrometer at ECN-Petten.[4] A schematic diagram of such a setup, together with the scattering diagram in reciprocal space, has been given in Fig. 1.

The neutron path was defined by 20′ horizontal collimation slits before the monochromator and

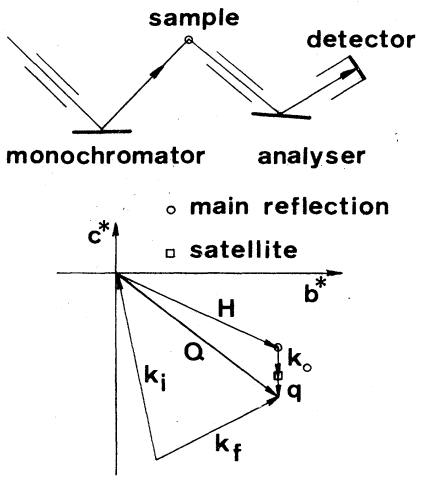

FIG. 1. Configuration of triple-axis spectrometer and corresponding scattering diagram in reciprocal space. The figure shows the definition of wave vectors.

before the analyzer. Vertical collimation before the monochromator was 1° and in the other parts of the spectrometer a few degrees. Bent pyrolytic graphite crystals, with a mosaic spread of about 35′ were used as monochromator and analyzer. Incoming energy could easily be chosen by setting the monochromator angle, which was kept constant during the energy scans. A 10-cm-thick pyrolytic graphite block, placed after the monochromator, removed second-order contamination. We used the filter for incoming energy of 12.3 meV as well as 5.5 meV because the available beryllium filter was too thick for optimum performance. However, the remainder of the second-order contamination in the beam does not interfere with our measurements. Neutrons of half the chosen wavelength could only give a spurious intensity at first-order satellite positions (near hkl), if there were strong second-order satellites at $2h2k2l$. As these do not exist, we can disregard the second-order neutrons.

We used an incoming energy of 12.3 meV to get a rough picture of the scattering; 5.5-meV neutrons were selected when high-energy resolution was required. The higher resolution has to be paid for with a fall in intensity by a factor of 10 compared with 12.3-meV neutrons. Consequently, rather long measuring times were needed: a typical energy scan took about 20 h. The spectrum of scattered neutrons is determined by varying the analyzer crystal setting. Thereby its reflectivity enters into the final intensity. This effect can be neglected, however, because of the limited energy ranges involved and the small energy dependence of the reflectivity. The sample was mounted in a furnace that kept the selected

temperature constant within 0.2°C. Absolute temperature is determined with a commercial chromel-alumel thermocouple, having an error of 1°C. Spectrometer angles are set by programming a computer that is online attached to the spectrometer. The furnace controller is also set by this computer.

Sample preparation

Crystals were grown at the Chemistry Department of the Technical University in Delft by slow evaporation of an aqueous solution of RbBr and $ZnBr_2$ at 40°C, which yielded single crystals with a volume of 3–7 cm^3. Unfortunately, the crystals contain small amounts of the solution. This is probably due to the large temperature dependence of the solubility, which causes irregular growth via slight temperature fluctuations. Consequently, we must heat the crystals very carefully to avoid rupture. Since the incoherent scattering is much higher than expected, we conclude that inclusions from the solution (i.e., the hydrogen) are responsible for the main part of the incoherent intensity.

III. THEORY

Neutron scattering can be used as a spectroscopic method which is especially powerful in the case of atomic vibrations at short wavelengths, i.e., wavelengths in the order of 10 Å and frequencies of about 10^{12} Hz. The fluctuations associated with a modulation phase transition are expected to be in this region both in the high- as well as in the low-temperature phase. Particularly in the high-temperature phase the fluctuations will have a frequency accessible for neutron spectroscopy, on condition that they correspond to small oscillations of the atoms. We assume such a critical mode in the high-temperature phase, and a distortion of the structure in the low-temperature phase which has the same polarization vector symmetry. Consequently, our model is that of a purely displacive modulation and the transition is of the order-order type. In contrast to this model, we have the possibility of disorder modulation as suggested for certain A_2BO_4 structures.[5] In the low-temperature phase the disorder type should be an occupation modulation, i.e., the probability of finding an atom in one out of a set of positions is modulated. Here, the critical mode corresponds to large jumps of the atoms. In general, the frequency of such a mode will be much lower than normal phonon frequencies.

On approaching the critical temperature from below, the displacive model predicts continuously decreasing amplitudes A_κ. The most important prediction of the model is the occurrence of diffraction harmonics, arising from a modulation of the phase of the atomic diffraction amplitudes. Neither of these features of the displacive model belong to disorder modulation. In practice, however, the distinction can be severely blurred. For instance, if the wave is anharmonic, second-order satellites will also occur in the disorder model. Moreover, a disorder mode could couple in a modulation wave to a displacive one.

The situation is even more complicated when considering the dynamics of the fluctuations in the high-temperature phase. Ideally, the displacive type corresponds to a soft-phonon model and a pseudospin model applies to the disorder type. This distinction is only relevant if the soft mode is underdamped or the tunneling frequency in the disorder case is low compared with normal oscillation frequencies. Between these extrema, we cannot distinguish the dynamical properties of the two models.

We will proceed now with a derivation of the structure factor for our model of a modulated structure, in the high- as well as in the low-temperature phase. Second, we will give a formula for the dynamic part of the structure factor, which will be applied in the high-temperature phase. These expressions do not represent a rigorous theory of a modulated crystal, but we use them to analyze our data in a phenomenological way. One should be aware that we give just those formulas that fit best to the experimental results.

Scattering cross section

The partial differential scattering cross section is given by:

$$\frac{d^2\sigma}{d\Omega d\omega} = \frac{k_f}{2\pi k_i} S(\vec{Q},\omega)$$

$$= \frac{k_f}{2\pi k_i} \int_{-\infty}^{\infty} dt e^{-i\omega t} \int d^3r G(r,t) e^{i\vec{Q}\cdot\vec{r}}$$

(k_f and k_i are final and initial wave vectors).

The scattering properties of a crystal are contained in the scattering law, $S(Q,\omega)$, through the density correlation function $G(r,t)$

$$G(r,t) = \int d^3r' \langle \rho(\vec{r},0)\rho(\vec{r}'+\vec{r},t)\rangle$$

with the scattering density

$$\rho(\vec{r},t) = \sum_i b_i \delta(\vec{r} - \vec{r}_i(t))$$

(b_i is the scattering length of the ith particle).

Defining $F(\vec{Q},t) = \sum_i b_i e^{i\vec{Q}\cdot\vec{r}_i(t)}$, the scattering law becomes

$$S(\vec{Q},\omega)=\int_{-\infty}^{\infty} dt e^{-i\omega t}\langle F(-\vec{Q},0)F(\vec{Q},t)\rangle .$$

These formulas are quite general and now we substitute our particular model of a lattice structure with displacive modulation

$$\begin{aligned}\vec{r}_{\kappa l}(t)&=\vec{r}_l+\vec{r}_\kappa+\vec{A}_{\kappa l}(t)\sin[\vec{k}_0\cdot\vec{r}_l+\phi_{\kappa l}(t)]\\&\simeq\vec{r}_l+\vec{r}_\kappa+\vec{A}_\kappa\sin(\vec{k}_0\cdot\vec{r}_l+\phi_\kappa)\\&\quad+\Delta\vec{A}_{\kappa l}(t)\sin(\vec{k}_0\cdot\vec{r}_l+\phi_\kappa)\\&\quad+\vec{A}_\kappa\Delta\phi_{\kappa l}(t)\cos(\vec{k}_0\cdot\vec{r}_l+\phi_\kappa)\end{aligned}$$

(in the last part A_κ and ϕ_κ stand for the average amplitude and phase, respectively).

Here the shifts of the atom positions, due to the amplitude and phase fluctuations, are written

$$\vec{U}_{\text{ampl}}(t)=\Delta\vec{A}_{\kappa l}(t)\sin(\vec{k}_0\cdot\vec{r}_l+\phi_\kappa),$$

$$\vec{U}_{\text{ph}}(t)=\vec{A}_\kappa\Delta\phi_{\kappa l}(t)\cos(\vec{k}_0\cdot\vec{r}_l+\phi_\kappa).$$

We introduce two different fluctuation modes, because the incommensurability of the lattice deformation (i.e., the irrationality of k_0) demands a description with a two-component order parameter: an amplitude and a phase.

Now we use the Jacobi-Anger transformation

$$e^{iZ\sin\phi}=\sum_m e^{im\phi}J_m(Z)$$

to expand the scattering amplitude $\exp[-i\,\vec{Q}\cdot\vec{r}_{\kappa l}(t)]$ in a product of sums of Bessel functions. In this product we retain the zeroth and first-order Bessel functions, which have the fluctuation amplitudes as argument. These can be approximated to first order in the argument and using a Fourier expansion of the fluctuation amplitudes

$$\Delta\vec{A}_{\kappa l}(t)=\sum_q u_q(t)\vec{\xi}_\kappa e^{i\vec{q}\cdot\vec{r}_l}$$

($\vec{\xi}_\kappa$ is the polarization vector),

$$\Delta\phi_{\kappa l}(t)=\sum_q \phi_q(t)e^{i\vec{q}\cdot\vec{r}_l},$$

we obtain the following expression for the scattering law

$$\begin{aligned}S(\vec{Q},\omega)&=\sum_m|F_B(\vec{Q})|^2\Delta(\vec{Q}+m\vec{k}_0)\\&\quad+\int dt\,e^{-i\omega t}\sum_{p=\pm1}\sum_q|F_{\text{ampl}}(\vec{Q})|^2\Delta(\vec{Q}+p\vec{k}_0-q)\\&\qquad\times\langle u_q(0)u_{-q}(t)\rangle\\&\quad+|F_{\text{ph}}(\vec{Q})|^2\Delta(\vec{Q}+p\vec{k}_0-q)\langle\phi_q(0)\phi_{-q}(t)\rangle .\end{aligned}\tag{2}$$

Where

$$F_B=\sum_\kappa b_\kappa e^{i\vec{Q}\cdot\vec{r}_\kappa}e^{im\phi_\kappa}J_m(\vec{Q}\cdot\vec{A}_\kappa),$$

$$F_{\text{ampl}}=\sum_\kappa b_\kappa e^{i\vec{Q}\cdot\vec{r}_\kappa}e^{i\phi_\kappa}(\vec{Q}\cdot\vec{\xi}_\kappa),$$

$$F_{\text{ph}}=\sum_\kappa b_\kappa e^{i\vec{Q}\cdot\vec{r}_\kappa}e^{i(\phi_\kappa+1/2\pi)}(\vec{Q}\cdot\vec{A}_\kappa),$$

$$\Delta(\vec{Q})=\sum_{h,k,l}\delta(\vec{Q}-h\vec{a}^*-k\vec{b}^*-l\vec{c}^*).$$

In this expression we have neglected the fourth-order terms in amplitude and phase fluctuations because they represent two-phonon processes. We also neglect the term of the form $\langle u_q\phi_{-q}\rangle$ because it will be small at small q (note that this cross term is not necessarily zero, since in general amplitude and phase modes cannot be associated with normal coordinates of the Hamiltonian). We see that the long-wavelength fluctuations of the order parameter are observable around first-order satellites. Furthermore, it is important for experimental reasons that both the phase and amplitude fluctuations are strong at positions where the satellite intensity is strong. This follows directly from the structure factors, which contain similar atomic scattering amplitudes in the case of Bragg reflections and amplitude and phase fluctuations. In particular, there is no way to distinguish between scattering from amplitude and phase modes by selecting different positions in reciprocal space. Although these modes are "out of phase," since one is represented by a sine and the other by a cosine function, the square of their structure factors is identical. In the high-temperature phase the static deformation wave vanishes and the amplitude fluctuations are identical with the soft mode fluctuations.

Relation to thermodynamics

In order to explain the relation between neutron scattering and thermodynamics, we shall employ a model of dipoles formed by shifted rigid ions with charges z_κ that represents a crystal with displacive fluctuations.[6] The polarization is

$$P(\vec{r},t)=\sum_{l,\kappa} z_\kappa\vec{U}_{l\kappa}(t)\,\delta(\vec{r}-\vec{r}_{l\kappa}),$$

with the Fourier transform

$$\hat{P}(\vec{Q},t)=F_d(\vec{Q})\hat{U}(\vec{q},t),$$

which we have written as a product of the normal coordinate of the displacement mode

$$\vec{U}_{l\kappa}(t)=m^{-1/2}\vec{\xi}_{\kappa q}\hat{U}(\vec{q},t),$$

and the dipolar structure factor:

$$F_d(\vec{Q}) = \sum_\kappa z_\kappa m_\kappa^{-1/2} \vec{\xi}_{\kappa q} e^{i\vec{\tau}\cdot\vec{r}_\kappa}, \quad \vec{Q} = \vec{\tau} + \vec{q}\,.$$

As a result, the correlation function of the polarization fluctuations can be expressed as a product of the dipolar structure factor and the correlation function of the normal coordinate. The neutron scattering cross section is proportional to this correlation function and thus the neutron scattering technique allows us to determine the generalized susceptibility of our system. From this point of view neutron scattering is a unique tool to study modulated crystals since the polarization fluctuations are inaccessible to dielectric techniques. Although neutron scattering is proportional to the response at a given wavelength and frequency of our crystal, it may be difficult to obtain the susceptibility because we must know the dipolar structure factor that relates a fluctuation in the atom positions to a polarization fluctuation.

The relation between the scattering law and the susceptibility is obtained as[6]

$$S(Q,\omega) = 2\upsilon \frac{|F(Q)|^2}{|F_d(Q)|^2} \frac{k_B T}{\omega} \chi''(q,\omega)$$

and

$$S(Q) \equiv \frac{1}{2\pi} \int_{-\infty}^{\infty} d\omega S(\vec{Q},\omega)$$

$$= \upsilon \frac{|F(Q)|^2}{|F_d(Q)|^2} k_B T \chi(q) \qquad (3)$$

(υ is the unit-cell volume).

$F(Q)$ is the structure factor of the soft mode. In the high-temperature phase, this is the structure factor of amplitude fluctuations and in the low-temperature phase it stands for the structure factor of both amplitude and phase modes.

Time dependence of fluctuations

It is possible to picture the critical fluctuations in the high-temperature phase as a soft phonon. In that case, our starting point for a treatment of the dynamics of the fluctuations is a harmonic oscillator. A damping mechanism has to be added in order to describe the situation near the phase transition. Hence, the equation of motion of the normal coordinate of the critical mode has the form[7-9]

$$\frac{\partial^2}{\partial t^2} \hat{U}(t) = -\omega_0^2 \hat{U}(t) - \int_0^t dt' M(t'-t) \times \frac{\partial}{\partial t'} \hat{U}(t') + F e^{i\omega t}. \qquad (4)$$

On the right-hand side there is, besides the restoring force, a rather exotic damping term; through the integral the damping depends on the previous velocities of the normal coordinates. An interpretation of this phenomenon is that the fluctuations in the critical mode perturb the thermal occupation numbers of the other modes. In turn, these modes influence the relaxation of the fluctuations. The function $M(t)$ describes the relaxation towards equilibrium: $M(t) = (\Gamma/t) \times \exp(-t/\tau)$. If the relaxation is fast, the integral in Eq. (4) can be reduced to a term $\Gamma(\partial/\partial t)\hat{U}(t)$ and a simple damped oscillator results. However, if τ^{-1} becomes lower than the harmonic frequency of the mode, there is an increasing response at low frequencies and a central peak appears in the spectrum. The response is

$$\chi(\omega) = \hat{U}/F = \frac{1}{\omega^2 + i\Gamma_{eff}\omega - \omega_0^2}$$

(with $\Gamma_{eff} = \Gamma/1+\omega^2\tau^2$),

$$S(\omega) \sim \frac{\chi''(\omega)}{\omega} = \frac{\Gamma_{\rm eff}}{(\omega_1^2 - \omega^2)^2 + (\Gamma_{\rm eff}\,\omega)^2}\,, \qquad (5)$$

$$\left(\omega_1^2 = \omega_0^2 + \frac{\omega^2\Gamma\tau}{1+\omega^2\tau^2}\right).$$

Again, the damped oscillator results if $\Gamma_{\rm eff}$ and ω_1 are frequency independent. The sum rule gives:

$$\int_{-\infty}^{\infty} d\omega\, S(\omega) \sim \frac{k_B T}{\omega_0^2}\,.$$

The wave-vector dependence can be incorporated in this model via ω_0^2. Writing

$$\omega_0^2 = a(T - T_c) + \sum_i \lambda_i q_i^2\,,$$

results in a scattering intensity of the form:

$$S(q) = \frac{F^2}{F_d^2} k_B T \chi(q) = \frac{F^2}{F_d^2} \frac{k_B T}{\omega_0^2}$$

$$= \frac{F^2}{F_d^2} \frac{k_B T}{a(T-T_c) + \sum_i q_i^2/\kappa_i^2}\,,$$

where $\kappa_i^2 = \omega_0^2/\lambda_i$. This form of the critical scattering in the high-temperature phase can also be derived from a Landau free energy[10] (as a function of a complex order parameter) that we write in terms of the Fourier components of the polarization:

$$\delta F_q = \tfrac{1}{2} a(T-T_c) P_q^2 + \tfrac{1}{4} C P_q^4 + \frac{1}{2} \sum \lambda_i q_i^2 P_q^2.$$

This yields for $T > T_c$

$$\chi(q) = \frac{1}{a(T-T_c) + \sum_i \lambda_i q_i^2}\,, \qquad (6)$$

and for $T < T_c$:

$$\chi(q) = \frac{1}{2(a|(T-T_c)|+\sum_i \lambda_i q_i^2)} .$$

IV. ANALYSIS OF SCATTERING PROFILES

For the measurement of phonon frequencies by means of a triple-axis spectrometer use is made of the scattering relations

$$\epsilon_i - \epsilon_f = \hbar\omega(q), \quad \vec{k}_i - \vec{k}_f = \vec{Q} = \vec{q} \pm \vec{\tau} .$$

A peak in the scattered intensity is observed when these laws of conservation of energy and (quasi) momentum are fulfilled. The width of the peak is partly determined by the window in $\vec{Q}$-ω space, related to the spectrometer configuration and setting. Cooper and Nathans[11] have calculated this window, or resolution function, assuming an ideal Gaussian dependence of the final intensity on the angle of incidence of the neutrons on crystals and Soller slits.

For a setting $(\vec{Q}_0, \omega_0)$ of the instrument, the detected intensity is

$$I(\vec{Q}_0, \omega_0) = \int\int d\vec{Q}\, d\omega R(\vec{Q} - \vec{Q}_0, \omega - \omega_0) F(\vec{Q}, \omega) , \tag{7}$$

where

$$R(\vec{Q}, \omega) = R(\vec{x}) = \exp\left(-\frac{1}{2}\sum_{k,l=1}^{4} m_{k,l} x_k x_l \ ;\right)$$

$F(\vec{Q}, \omega)$ is an intrinsic cross section. Only the off-diagonal elements of $\vec{m}$ in the vertical direction are zero. For most functions $F(\vec{Q}, \omega)$ the convolution of Eq. (7) cannot be solved analytically. Therefore, we calculated the integral numerically, using a program[12] based on the formulas given by Cooper and Nathans. The intrinsic cross section normally contains adjustable parameters that must be obtained from a fit to the measured profiles. In general, however, refinement of the parameters in $F(\vec{Q}, \omega)$ is thwarted, because of the length of the calculation of the folding integral.

Two solutions have been chosen to avoid this problem; approximating the integral by assuming that $F(\vec{Q}, \omega)$ is independent of Q or calculating the convolution for a set of parameters and interpolating to find the best set. In order to check the results of the convolution program we made energy scans of the incoherent scattering of vanadium at incoming energy of 12.3 and 5.5 meV. The measured resolution widths at these energies amount to 0.9 meV (0.22 THz) and 0.24 meV (0.058 THz), respectively, and agree within 10% with the calculated values. This latter value will be taken as the accuracy with which the resolution of the spectrometer is known.

Since the incoherent scattering is independent of $\vec{Q}$ we can set an upper limit to the width of a peak around $\omega = 0$ due to elastic scattering. Close to the transition temperature the situation is complicated because of the $\vec{Q}$ dependence of the scattering. We notice that this can only result in a narrowing of the spectrum. Narrowing is due to the elongation of the resolution ellipsoid, defined by

$$\sum m_{k,l} x_k x_l = \ln 2$$

in Q-ω space. In this way one can tell whether the observed scattering has to be attributed to static fluctuations, or that dynamic effects are needed to explain the spectra.

V. RESULTS AND DISCUSSION

Static behavior

The most direct evidence for the transition is the vanishing of the satellite reflections on approaching the critical temperature. In our model the loss of long-range order is caused by diverging fluctuations in the phases and amplitudes of the atom shifts. However, the decrease of the satellite intensity is mainly due to a decreasing amplitude of the modulation wave. This amplitude is just the static part of the critical mode.

The amplitude may be taken as the modulus of the order parameter and is obtained from the square root of the intensity of a satellite. Assuming that the mean phases, contained in the polarization vectors $\vec{\xi}_\kappa$, are temperature independent then we have

$$[I(T)]^{1/2} \sim |\langle A^{\mathrm{crit}}_{\vec{k}_0}(T)\rangle| .$$

Figure 2 shows the intensity of the (0211) reflection as a function of temperature. It can be seen that, in agreement with the above, apart from diffuse scattering, the scattered intensity and hence the order parameter goes to zero continuously. Following the argument in Sec. I it is of crucial importance whether the diffraction pattern contains second-order satellites, or not. Although observing higher-order satellites was as yet unsuccessful with x-rays, they have been found with neutron scattering.

Close to the strong (0211) satellite, we located the (022$\bar{2}$) satellite. This suggests that we deal here with the purely displacive-type modulation, because a crystal with disorder modulation has

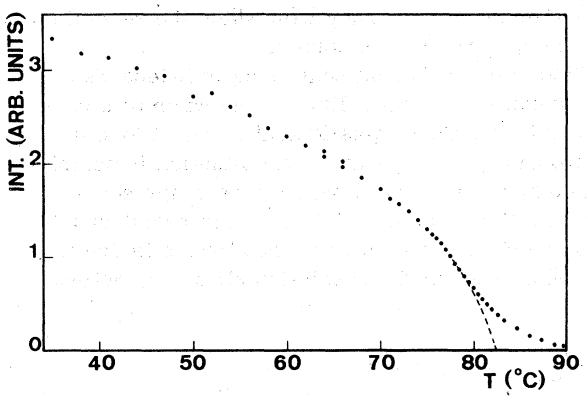

FIG. 2. Satellite intensity as a function of temperature. Measurement without analyzer.

no second-order satellites in the diffraction pattern. However, we cannot rule out the possibility of an anharmonic wave. That would also give rise to second-order satellites even in the case of disorder modulation. Of course, a decision can only be made after a full structure analysis, which is in progress, has been completed.

Anyhow, an important test of the model of the modulation is the temperature dependence of the $(022\bar{2})$ reflection. Figure 3 shows that $I^2_{022\bar{2}}$ follows the temperature dependence of $I^2_{022\bar{1}}$, in accordance with the structure factors (2):

$$F_{022\bar{2}} \sim J_2(\vec{Q}\cdot\vec{A}) \approx (\vec{Q}\cdot\vec{A})^2 ,$$

$$F_{022\bar{1}} \sim J_1(\vec{Q}\cdot\vec{A}) \approx \vec{Q}\cdot\vec{A} .$$

In the same figure, we plotted the temperature dependence of two first-order satellites. The similarity of their temperature dependence supports our model of a decreasing amplitude for all atoms and constant phases. The quotient of the satellite intensities is:

$$I_{0211}/I_{022\bar{1}}/I_{022\bar{2}} = 3000/12/11 \text{ (in counts/sec)}$$

at room temperature.

The diffuse scattering, centered around the satellite position, peaks at the critical temperature since it is directly proportional to the susceptibility.

In Fig. 4(a) the intensity around the satellite position is shown at several temperatures. The diffuse scattering is sharper in the direction perpendicular to $\vec{k}_0$, than parallel to $\vec{k}_0$. This means that the correlations are strongest in planes parallel to the wave front.

In Fig. 4(b) the inverse intensity, at $\vec{q}=0$, is plotted as a function of temperature, showing a linear relationship in agreement with the Curie-Weiss law. In the low-temperature phase we

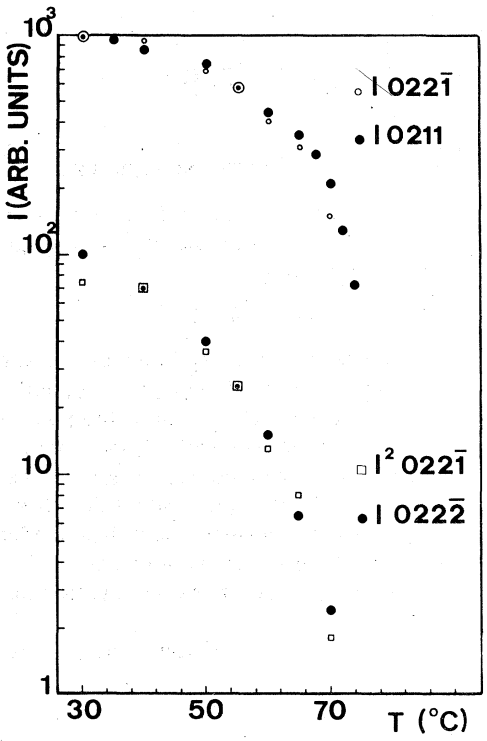

FIG. 3. Temperature dependence of first- and second-order satellites. Note the logarithmic scale. An arbitrary scale factor has been applied for comparing the results.

must separate Bragg scattering from the total intensity. For this procedure we describe the satellite intensity as

$$I_{0211} \sim |T - T_c|^{2\beta} . \tag{8}$$

We obtained $\beta = 0.30$ from a fit to the data in Fig. 2. T_c was determined independently as the temperature where the diffuse intensity at $\vec{q} = 0.063\vec{c}^*$ peaks. Using Eq. (8) in the vicinity of T_c, we can subtract the Bragg scattering, yielding the diffuse intensity. In Fig. 5, we plotted the diffuse intensity at $\vec{q} = 0.063\vec{c}^*$ from the satellite position. The Bragg part is drawn following the before mentioned procedure. The inverse intensity at $\vec{q} = 0.063\vec{c}^*$ is shown in Fig. 6 as a function of temperature and the relation of Eq. (6) is fulfilled, although only in a small region around the transition. The quotient of the Curie constants in the high- and low-temperature phase (C_h and C_l) is $C_h/C_l = 0.52$. Far above T_c the intensity decreases much steeper than predicted by the Curie-Weiss law.

At $q=0$, the statistical error in the diffuse scattering below T_c is rather large due to the enormous contribution of Bragg scattering to the total intensity. Therefore, we can measure dif-

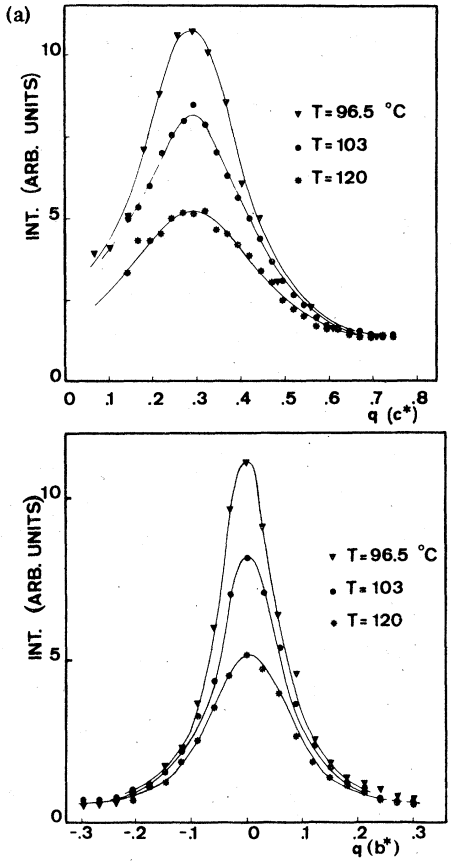

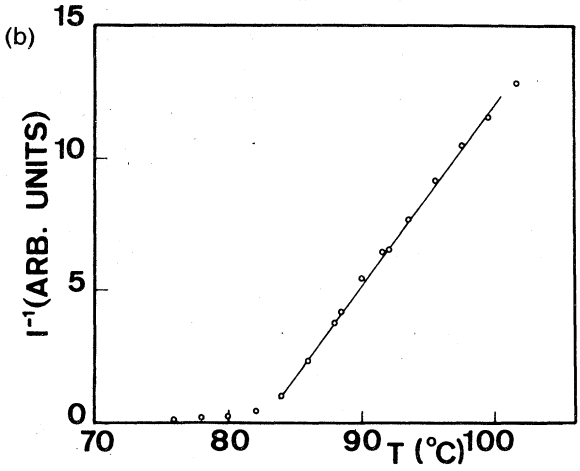

FIG. 4. (a) Diffuse intensity distribution along the c^* and b^* axes. The correlation lengths at $T=120\,^{\circ}\mathrm{C}$ are: $\kappa_c = 0.194\ \text{Å}^{-1}$ and $\kappa_b = 0.112\ \text{Å}^{-1}$. (b) Inverse intensity of diffuse scattering at $q=0$, as a function of temperature.

fuse scattering in a small temperature interval below T_c, only. Here we get $C_h/C_l = 0.45$.

The exponent that we use to fit the decreasing intensity of the satellite, on approaching T_c, to a power law, can be identified with the exponent of the order parameter. Since measurements with a much smaller crystal resulted in a higher value of β ($\beta = 0.38$), we think that the present results suffer from secondary extinction. Extinction attenuates strong reflections relatively more than the weaker ones, and thus influences the exponent β. Therefore, we will neglect at present the discrepancy between the experimental value and the mean-field value of $\beta = \frac{1}{2}$.

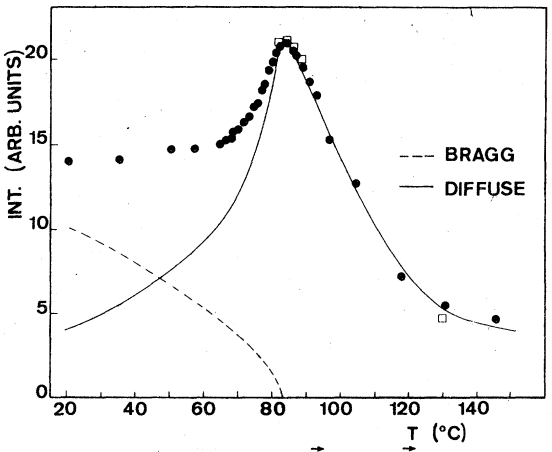

FIG. 5. Diffuse intensity at $\vec{q}=0.063\ \vec{c}^*$ from the satellite position 0211. The procedure for the subtraction of Bragg scattering is explained in the text.

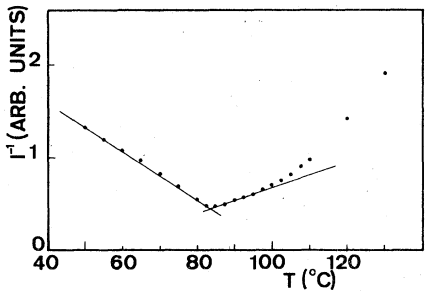

FIG. 6. Inverse intensity at $\vec{q}=0.063\ \vec{c}^*$ as a function of temperature.

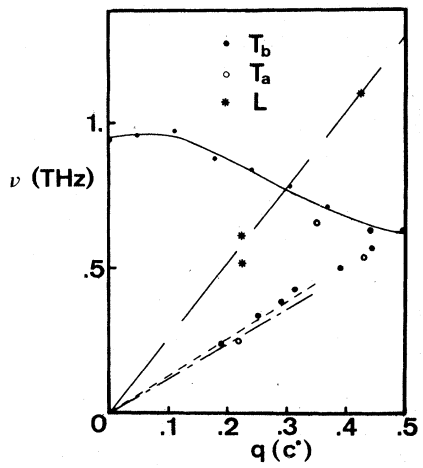

FIG. 7. Acoustical phonon branches and one optical branch in the c direction. Dashed lines represent ultrasonic velocities. T_b: transverse b polarized, T_a: transverse a polarized, L: longitudinal. Here, the wave vector q is measured from a main reflection.

As explained, we derived T_c from the peaking of diffuse scattering as a function of temperature. A problem arose here, because we found considerable deviations of T_c in different crystals. Values of T_c ranged from 78.0 to 82.5°C; a possible cause of these differences is the static disorder, which might be present in the crystals. If the concentration of defects differs for our crystals, it could have an influence on the values of T_c. In the analysis we scaled all results to a T_c of 82.5°C.

Dynamics of modulated phase

The dynamical aspects of modulated Rb_2ZnBr_4 were studied between room temperature and T_c. This choice was made for experimental convenience although at 20°C the modulation has not reached its ground state. From Fig. 2, it is clear that the amplitude of the wave would be larger at lower temperatures. Also, a neutron-diffraction powder diagram obtained at helium temperature showed much stronger satellites compared to room-temperature data. The effect of the modulation on the dynamics of the crystal and the observability of possible new excitations might depend on the amplitude. Thus, we have to be reluctant in drawing conclusions from our measurements about the modulation ground state. Figure 7 shows the acoustical branches and one optical branch in the $\vec{c}$ direction. The slope of the acoustical branches, for small $\vec{q}$, is in good agreement with the elastic constants from ultrasound measurements.[13] Note that the frequencies are quite low, which reflects the softness of the material. We estimate the Debye temperature from the elastic constants (in Table I), yielding

$$\Theta_D = (h/k_B)[(9/4\pi V_A)\langle C\rangle^3]^{1/3} \approx 100 \text{ K}.$$

Here, h/k_B is the thermal energy per atom, and V_A is the volume per atom, and $\langle C\rangle$ is the mean velocity of sound. The value is in good agreement with the low melting temperature of 470°C. According to the Lindeman melting formula the Debye temperature follows from the melting temperature as

$$\Theta_D = 120\bar{A}^{-5/6}\rho_0^{1/3}T_M^{1/2}$$

($\bar{A}$ is the mean atomic weight, ρ_0 is the density)

$$\Theta_D \approx 105\,K \text{ with } \bar{A} = 79.9 \text{ and } \rho_0 = 3.72 \text{ g/cm}^3.$$

The pseudohexagonality of the structure is reflected in the approximate equality of C_{11}, C_{22}, and C_{44}, C_{55}. This follows from the isotropy of the ultrasonic velocity perpendicular to a hexagonal rotation axis.

From a preliminary crystallographic study it was concluded that the atom shifts are in the b direction. So, we expect the soft mode to have this polarization. As explained before, one is unable to measure the complete set of dispersion branches.

On the other hand, we found a rather low-lying branch with the required polarization. This is the optical branch (see Fig. 7) that is degenerate with the acoustical b-polarized branch at the Z point. No abnormal temperature dependence of this branch was detected, which is in contrast to the results of a neutron-diffraction study of the isostructural compound K_2SeO_4. For this compound, Iizumi *et al.*[14] report a softening of the branch at a modulation phase transition that is characterized by $k_0 = 0.31c^*$. Thus, one has to conclude that although both compounds have the same symmetry and belong to the same class of modulated crystals, the exact mechanism of their incommensurate structural transitions is different. Of course, there are other branches, besides the one shown in Fig. 7, that may soften in Rb_2ZnBr_4. The temperature dependence of the velocity of sound, obtained by neutron scattering and ultrasonic measurements is shown in Fig. 8. The frequency of the branch as a function of tem-

TABLE I. Elastic constants of Rb_2ZnBr_4 on orthorombic pseudohexagonal axes. Data from ultrasonic measurements (Ref. 13). Units of 10^{11} dyn/cm^2 (accuracy ±1%).

$C_{11} = 1.80$	$C_{44} = 0.554$
$C_{22} = 1.64$	$C_{55} = 0.500$
$C_{33} = 2.22$	$C_{66} = 0.332$

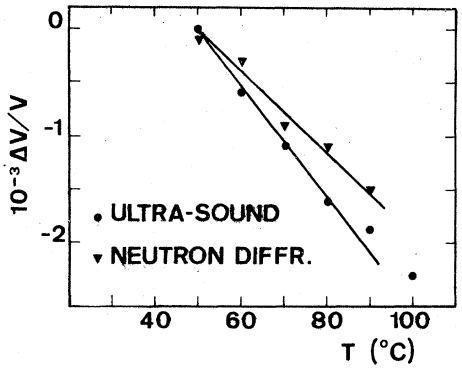

FIG. 8. Relative change of the transverse b polarized velocity of sound in the c direction vs temperature, as determined, respectively, by the ultrasonic and the neutron scattering technique.

perature was also measured at other points in the Brillouin zone, where it showed the same temperature dependence. The linewidth of the phonons is rather large (i.e., a full width at half maximum of .08 THz at a frequency of 0.2 THz). but temperature independent (i.e, from 20 to 200°C).

In view of the irrationality of the modulation wave vector, the phase of the modulation wave in the structure is arbitrary. Consequently there is a mode with vanishing frequency at the modulation wave vector,[15] corresponding to phase fluctuations at long wavelengths. Thus, the phase fluctuations should behave approximately as an "acoustic" branch. In this branch the phase fluctuations have a long wavelength, but the atom shifts are at short wavelengths. In the modulated phase, we analyzed the diffuse scattering that is shown in Fig. 5. The spectrum at $q=0.245c^*$ from the satellite, shown in Fig. 9, can be seen to exist of a sharp peak and broad wings. Subtracting the incoherent scattering results in a weak two-peak structure (Fig. 10). We emphasize that this form of the spectrum is due to a broadening of the uncorrected peak with respect to the spectrometer resolution. Clearly, the exact form of the resulting spectrum is critically dependent on the amount of subtracted incoherent intensity. Therefore, the accuracy of the profiles in Fig. 10 is low, and one can say at most that an overdamped excitation is present around the satellite position.

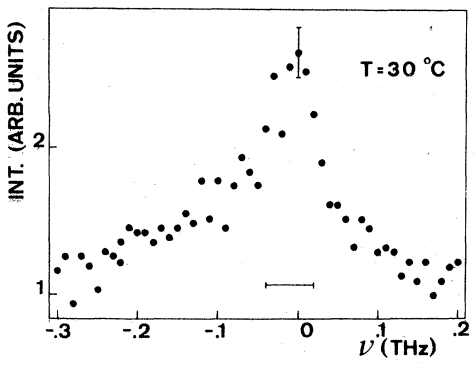

FIG. 9. Quasielastic energy scan (raw data) at room temperature at $q=0.245c^*$; the vector $\vec{q}$ is measured from the satellite position 0211. The bar indicates the resolution width.

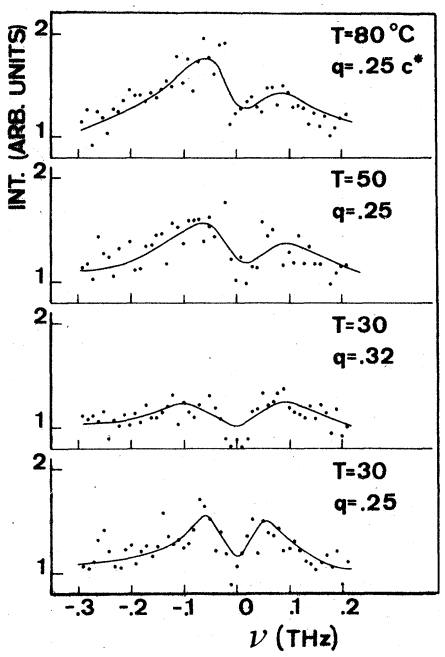

FIG. 10. Spectra of diffuse scattering around the satellite position 0211 at temperatures below T_c.

In Sec. III it was shown that amplitude or phase fluctuations of the order parameter cause inelastic scattering around the satellites, so we draw the conclusion that these excitations are overdamped in Rb_2ZnBr_4. Consequently, it is impossible to say that the weak peaks in Fig. 10 are due to a phason branch. At higher-energy transfers, we have not observed any other branches, corresponding to a propagating soft mode in the low-temperature phase.

Dynamics of high-temperature phase

Close to the critical temperature, the energy scans near the satellite position showed no peaks pointing to a soft excitation. That leaves the width of the bell-shaped curves as their only relevant feature. Adopting a purely static picture of the fluctuations, i.e., relative to neutron scattering resolution, we notice that the incoherent width is the upper limit for a peak in reciprocal space. We found a width in excess of the incoher-

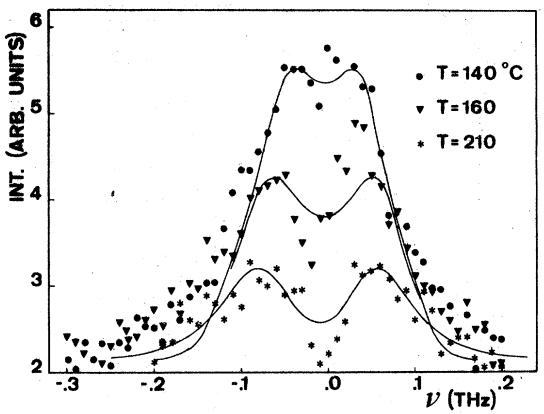

FIG. 11. Spectra of diffuse scattering at several temperatures above T_c, and at $q=0$. The curves are fits of a damped-harmonic-oscillator model.

ent width, even close to the critical temperature. Thus, we conclude that the fluctuations have an observable energy width, and that the critical mode is overdamped. Formula (5) should give an approximate description of the scattering, with a large damping constant. We analyzed our spectra with the help of this formula. Comparison of the observed and calculated spectra was made by calculating the convolution integral [see Eq. (7)]. At higher temperatures we could neglect the Q dependence of the scattering which greatly simplified the numerical calculation procedure which is needed for the evaluation of the convolution.

Above 140°C a two-peak structure is observed (Fig. 11) after subtraction of incoherent scattering. Clearly, the frequency of the soft excitation is only slightly temperature dependent, in contrast to most structural phase transitions. We still think it useful to analyze the scattering on the basis of expression (5) because it is generally valid, irrespective of the microscopic forces driving the phase transition.

For the scans with a two-peak structure we tried a fit with the harmonic frequency, a damping constant, and a proportionality factor as parameters. It turned out that in this way the best description was given by a temperature-dependent damping and a constant ω_0. This result shows the limited validity of a description with one damping mechanism, because a decreasing ω_0 should account for the increase of the intensity.

As a second try, we determined the proportionality factor to obtain a good description at $T = 210$ °C, where the fluctuations become underdamped. A fit of scans at several temperatures with ω_0 and Γ as parameters yielded a constant Γ. The increase of the integrated intensity was described by a fall of ω_0 over a temperature interval of 80 to 310 °C, with an accuracy of 15%. However, significant discrepancies occurred at the wings of the peaks. In our model this means that the relaxation is more complicated. Figure 11 shows the results of the fits at temperatures 140, 160, and 210 °C.

So far, we have only discussed here the inaccuracy in ω_0, due to discrepancies of the corrected data with our model. However, an important source of error in ω_0 may come from the subtraction of the incoherent scattering, which cannot be measured at the satellite position. In our case the incoherent scattering was determined after rotating the sample plus and minus 30° away from the satellite position around the axis perpendicular to the scattering plane. Although the incoherent scattering is principally independent of the sample orientation, geometrical effects may give rise to inaccuracies. These have a severe effect on ω_0 because subtracting too much incoherent intensity enhances the two-peak structure, thus makes the spectrum more underdamped. In that case a large error results in the deduced value of ω_0 since it is strongly correlated with the damping. Moreover, from an overdamped spectrum that shows only one peak (around $\omega=0$), it is even impossible to determine ω_0 and Γ independently. Therefore, the uncertainty in our value of ω_0 is large; but on the other hand we think that in view of the observed temperature dependence of the width of the spectra, the deduced value of ω_0 at 210 °C should be about equal to the half-width of the spectrum which is about 0.1 THz.

At a temperature of 90 °C, we made energy scans at various distances (q values) from the satellite position. A q-dependent width is observed that can be interpreted either as a q-dependent relaxation time of the fluctuations or as a dispersion of the soft branch. From Fig. 12, it can be seen that there is weak evidence for a splitting of the peak at $q=0.1c^*$, so the soft-mode description seems to be most adequate for these profiles. Figure 12 shows a fit to the data at 90 °C of the simple damped oscillator cross section. A significant discrepancy shows up at larger-energy transfers, possibly due to a complicated damping. Writing the damping as: $\Gamma(\omega)=\Gamma'+\Gamma''/(1+i\omega\tau)$, a better fit may be obtained. In this model, there is a central peak which gives together with the phonon part a good description of the $q=0$ spectrum, but deviates from the measured profile at $q=0.11c^*$. Thus, the damped harmonic oscillator model with a frequency-dependent damping can explain the changes from a more or less underdamped to an overdamped soft phonon. This change is

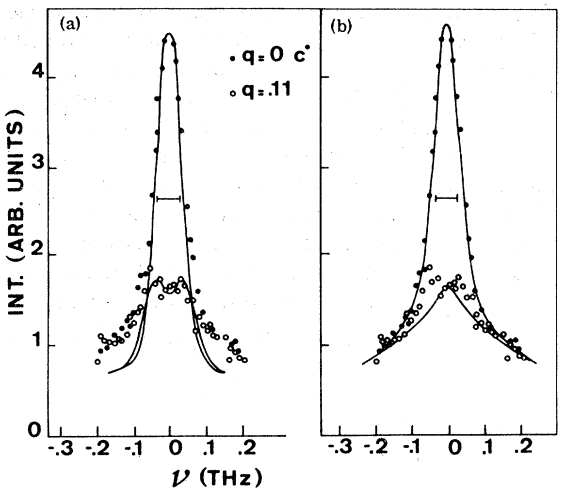

FIG. 12. (a) Spectra of diffuse scattering at $T = 90\,^{\circ}C$ at two values of q. The bar indicates the resolution width. Simple damped oscillator model fits are represented by the drawn curves. (b) Same data fitted to the model that contains a central peak feature.

brought about by a decreasing harmonic frequency and an increasing relaxation time of the critical mode to all other modes. In Fig. 13, the mean square of the harmonic frequency is plotted as a function of temperature.

The two sets of points are obtained by numerical integration, using the sum rule, and a fit to the damped harmonic oscillator model. Scaling is done at a temperature of 210 °C, where the splitting is best observed. Near T_c we observe a linear relationship, but large deviations occur far above the transition temperature.

In Sec. I, we mentioned the possibility of an order-disorder transition. Our reluctance to describe the fluctuations in the high-temperature

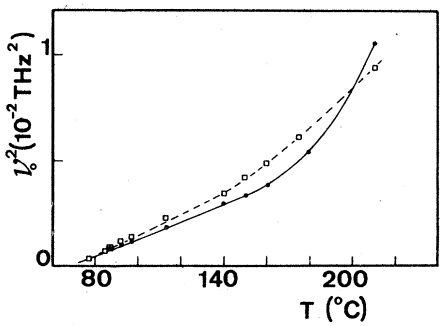

FIG. 13. Square of the harmonic frequency of the soft mode as a function of temperature. The squares represent data from a fit to a damped harmonic oscillator model and the dots are obtained from numerical integration of the spectra using the sum rule. The two sets of data were scaled at a temperature of 210 °C.

phase as a soft phonon stems from the overdamped inelastic profiles. Although a disorder model could fit the observations, we choose the soft-mode description in view of the splitting up of the spectra at high temperature. We admit, however, that in a large temperature region (about $\frac{1}{4} T_c$) above T_c, it is impossible to distinguish between the two descriptions. The frequency of the critical fluctuations is very low in this temperature interval but the amplitude is still too small, compared with the thermal vibration amplitude, to form a static deformation wave. The transition temperature will be determined by the decrease of the thermal vibration amplitude as a function of temperature. In this sense we may speak of an order-disorder transition because the thermal fluctuations determine the transition, whereas the mode has softened at a much higher temperature.

VI. CONCLUSIONS

From our findings we developed a picture of the modulation phase transition that fits in the soft-mode model. Even at high temperature ($T = 200\,^{\circ}C$), the Rb_2ZnBr_4 lattice is unstable for displacements with a wave vector of $k = 0.29c^*$. This critical mode has a low frequency, but on lowering the temperature the amplitude becomes only slowly large enough to form a static deformation wave. In other words: the mode becomes static when the thermal vibration amplitude of the atoms is comparable in size to the amplitude of the critical mode. When the crystal is in the normal phase, we see that the wave is rather uncorrelated, in space as well as in time, which follows from the broad scattering distributions in reciprocal space and frequency. In the low-temperature phase a Bragg peak appears and the displacement wave becomes static. Small fluctuations are still possible and according to the Goldstone theorem[15] one branch has a vanishing frequency at the satellite.

Below T_c we have found some evidence of diffuse scattering around the satellite which is broadened in frequency, but we were not able to find a well-defined soft branch in the low-temperature phase. Further experiments at low temperature will be needed to clarify this point. The experimental results are in reasonable agreement with the Landau theory of second-order phase transitions. Concerning the exponent of the order parameter, we will have to do an experiment with a very small crystal, in order to exclude any influence from secondary extinction on the value of β.

As a general remark, we must add that the crystals that we studied are far from perfect: from the anomalously high Debye-Waller factor we infer the presence of static imperfections. In our

analysis the imperfections are neglected, although it is well known that the dynamics of the transition is modified with respect to a perfect crystal. In view of our study, we think that our approach offers a first-order approximation which can be refined, by including imperfections, to give a better description of the real crystal without changing the fundamental concepts of the model that we employed.

ACKNOWLEDGMENTS

The authors wish to thank J. D. Axe, C. M. Fortuyn, F. Tuinstra, and P. M. de Wolff for stimulating discussions and numerous useful comments. H. Bronkhorst and J. van der Linden are gratefully acknowledged for growing the single crystals. One of the authors (C.J.P.) thanks the Physics Department, ECN, Petten for the hospitality during the experimental work. The authors thank W. v.d. Gaauw for his skillful technical assistance. This work is part of the research program of the Stichting voor Fundamenteel Onderzoek der Materie (F.O.M.) and has been made possible by financial support from the Nederlandse Organisatie voor Zuiver Wetenschappelijk Onderzoek (Z.W.O.).

[1]P. M. de Wolff, Acta Crystallogr. 30, 777 (1974).
[2]C. M. Fortuin, Physica (Utr.) A 86, 224 (1977).
[3]W. van Aalst, J. den Hollander, W. J. A. M. Peterse, and P. M. de Wolff, Acta Crystallogr. Sect. B 32 47 (1976).
[4]J. Bergsma, Reactor Centrum Nederland, Report No. RCN-121 (1970) (unpublished). J. Bergsma and C. van Dijk, Nucl. Instrum. Methods 51, 357 (1967).
[5]A. J. Berg, F. Tuinstra, and J. Warczewsky, Acta Crystallogr. B 29, 586 (1973).
[6]W. Cochran, Adv. Phys. 18, 157 (1969).
[7]F. Schwabl, Phys. Rev. Lett. 28, 500 (1972).
[8]R. Blinc and B. Zeks, *Soft Modes in Ferro-electrics and Antiferro-electrics* (North-Holland, Amsterdam, 1974).
[9]S. M. Shapiro, J. D. Axe, G. Shirane, and T. Riste, Phys. Rev. B 6, 4332 (1972). [These authors use a slightly different form of $S(\omega)$].
[10]M. A. Krivoglaz, *Theory of X-ray and Thermal-Neutron Scattering by Real Crystals* (Plenum, New York, 1969).
[11]M. J. Cooper and R. Nathans, Acta Crystallogr. 23, 357 (1967).
[12]E. J. Samuelsen, *Structural Phase Transitions and Soft Modes*, edited by E. J. Samuelsen, E. Andersen, and J. Feder (Universiteitsforlaget, Oslo, 1971).
[13]C. J. de Pater and R. A. Aptroot (unpublished).
[14]M. Iizumi, J. D. Axe, G. Shirane, and K. Shimaoka, Phys. Rev. B 15, 4392 (1977).
[15]T. Schneider and P. F. Meier, Physica (Utr.) 67, 521 (1973).